jove

High-resolution Neutron Spectroscopy to Study Picosecond-nanosecond Dynamics of Proteins and Hydration Water

Kevin Pounot[1,2], **Markus Appel**[2], **Christian Beck**[1,2], **Martin Weik**[3], **Giorgio Schirò**[3], **Yann Fichou**[4], **Tilo Seydel**[2], **Frank Schreiber**[1]

[1] Institut für Angewandte Physik, Universität Tübingen [2] Institut Max von Laue - Paul Langevin (ILL) [3] Institut de Biologie Structurale, Université Grenoble Alpes [4] Institut Européen de Chimie et Biologie, Bordeaux INP, Chimie et Biologie des Membranes et des Nanoobjets (CBMN), Université de Bordeaux

Corresponding Author

Kevin Pounot
kevin.pounot@uni-tuebingen.de

Citation

Pounot, K., Appel, M., Beck, C., Weik, M., Schirò, G., Fichou, Y., Seydel, T., Schreiber, F. High-resolution Neutron Spectroscopy to Study Picosecond-nanosecond Dynamics of Proteins and Hydration Water. *J. Vis. Exp.* (182), e63664, doi:10.3791/63664 (2022).

Date Published

April 28, 2022

DOI

10.3791/63664

URL

jove.com/video/63664

Abstract

Neutron scattering offers the possibility to probe the dynamics within samples for a wide range of energies in a nondestructive manner and without labeling other than deuterium. In particular, neutron backscattering spectroscopy records the scattering signals at multiple scattering angles simultaneously and is well suited to study the dynamics of biological systems on the ps-ns timescale. By employing D_2O-and possibly deuterated buffer components-the method allows monitoring of both center-of-mass diffusion and backbone and side-chain motions (internal dynamics) of proteins in liquid state.

Additionally, hydration water dynamics can be studied by employing powders of perdeuterated proteins hydrated with H_2O. This paper presents the workflow employed on the instrument IN16B at the Institut Laue-Langevin (ILL) to investigate protein and hydration water dynamics. The preparation of solution samples and hydrated protein powder samples using vapor exchange is explained. The data analysis procedure for both protein and hydration water dynamics is described for different types of datasets (quasielastic spectra or fixed-window scans) that can be obtained on a neutron backscattering spectrometer.

The method is illustrated with two studies involving amyloid proteins. The aggregation of lysozyme into µm sized spherical aggregates-denoted particulates-is shown to occur in a one-step process on the space and time range probed on IN16B, while the internal dynamics remains unchanged. Further, the dynamics of hydration water of tau was studied on hydrated powders of perdeuterated protein. It is shown that translational motions of water are activated upon the formation of amyloid fibers. Finally, critical steps in the protocol are discussed as to how neutron scattering

is positioned regarding the study of dynamics with respect to other experimental biophysical methods.

Introduction

The neutron is a charge-less and massive particle that has been successfully used over the years to probe samples in various fields from fundamental physics to biology[1]. For biological applications, small-angle neutron scattering, inelastic neutron scattering, and neutron crystallography and reflectometry are extensively used[2,3,4]. Inelastic neutron scattering provides an ensemble-averaged measurement of the dynamics without requiring specific labeling per se, and a signal quality that does not depend on the size or the protein[5]. The measurement can be done using a highly complex environment for the protein under study that mimics the intracellular medium, such as a deuterated bacterial lysate or even *in vivo*[3,6,7]. Different experimental setups can be used to study the dynamics, namely i) time-of-flight-giving access to sub-ps-ps dynamics, ii) backscattering-giving access to ps-ns dynamics, and iii) spin-echo-giving access to dynamics from ns to hundreds of ns. Neutron backscattering makes use of the Bragg's law $2d \sin\theta = n\lambda$, where d is the distance between planes in a crystal, θ the scattering angle, n the scattering order, and λ the wavelength. The use of crystals for backscattering toward the detectors allows for achieving a high resolution in energy, typically ~0.8 μeV. To measure the energy exchange, either a Doppler drive carrying a crystal in backscattering is used to define and tune the incoming neutron wavelength[8,9,10] (**Figure 1**), or a time-of-flight setup can be used at the cost of a decrease in energy resolution[11].

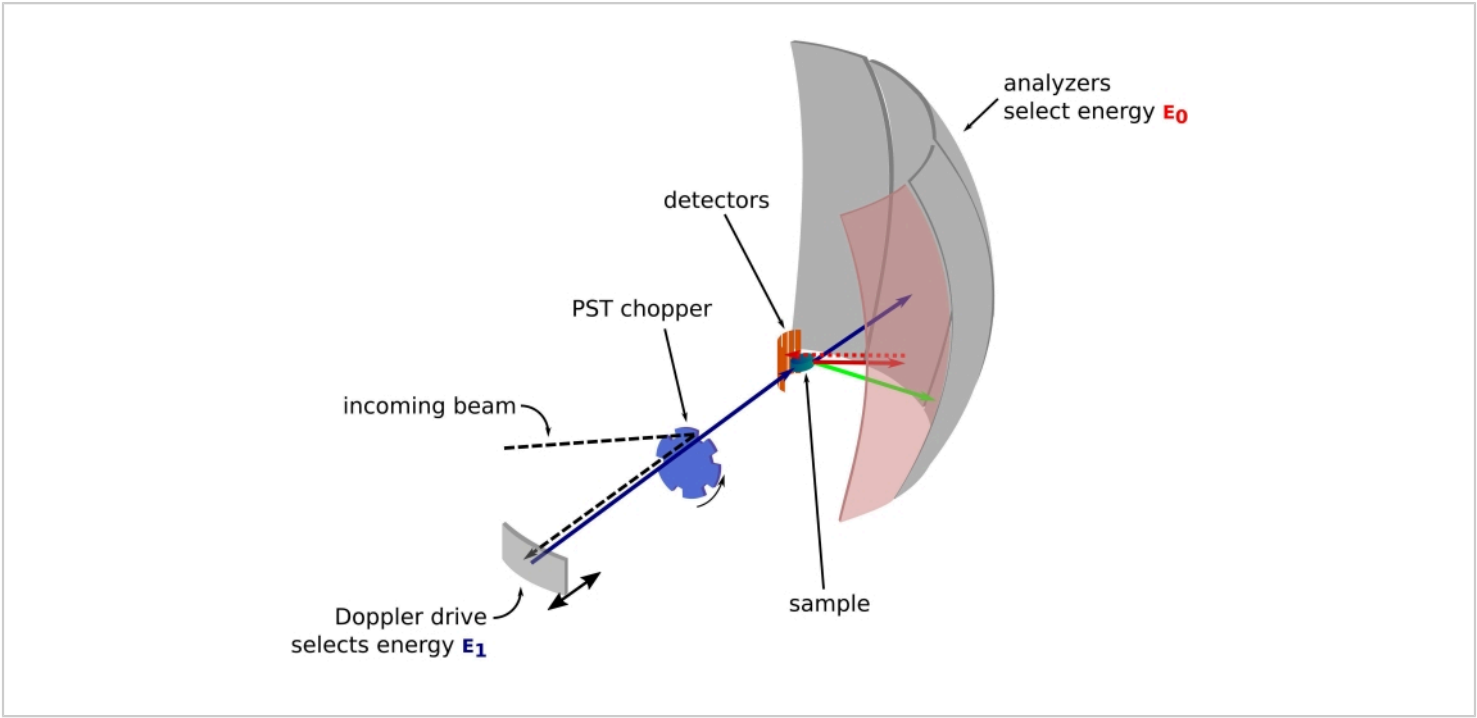

Figure 1: Sketch of a neutron backscattering spectrometer with a Doppler drive. The incoming beam hits the phase space transformation (PST) chopper[42], which increases the flux at the sample position. It is then backscattered towards the sample by the Doppler drive, which selects an energy E_1 (cyan arrow). The neutrons are then scattered by the sample (with different energies represented by the color of the arrows) and the analyzers, made of Si 111 crystals, will only backscatter neutrons with a specific energy E_0 (red colored arrows here). Hence, the momentum transfer **q** is obtained from the detected position of the neutron on the detector array, and the energy transfer is obtained from the difference E_1- E_0. The time-of-flight expected for the neutron pulse produced by the PST is used to discard the signal from the neutrons scattered directly toward the detector tubes. Abbreviation: PST = phase space transformation. Please click here to view a larger version of this figure.

For backscattering spectroscopy, the main contribution to the signal from hydrogen proton-rich samples, such as proteins, comes from incoherent scattering, for which the scattering intensity $S_{inc}(\mathbf{q}, \omega)$ is shown by Eq (**1**)[12]

$$S_{inc}(\mathbf{q},\omega) = \frac{\sigma_{inc}}{4\pi}\frac{k'}{k}\frac{1}{2\pi\hbar}\int_{-\infty}^{\infty}\left\langle e^{\mathbf{q}\mathbf{r}_j(0)}e^{\mathbf{q}\mathbf{r}_j(t)}\right\rangle e^{i\omega t} \quad (\mathbf{1})$$

Where σ_{inc} is the incoherent cross-section of the element considered, k' is the norm of the scattered wavevector, k the norm of the incoming wavevector, **q** (= k - k') the momentum transfer, $\mathbf{r_j}(t)$ the position vector of atom j at time t, and ω the frequency corresponding to the energy transfer between the incoming neutron and the system. The angular brackets denote the ensemble average. Hence, incoherent scattering probes the ensemble-averaged single-particle self-correlation of atom positions with time and gives the self-dynamics averaged over all atoms in the system and different time origins (ensemble average). The scattering function is the Fourier transform in time of the intermediate scattering function I(**q**, t), which can be viewed as the Fourier transform in space of the van Hove correlation function shown by Eq (**2**):

$$G(\mathbf{r},t) = \frac{1}{N}\int d\mathbf{r}'\,\langle\rho(\mathbf{r}'-\mathbf{r},0),\rho(\mathbf{r},t)\rangle \quad (\mathbf{2})$$

Where ρ(***r***,***t***) is the probability density of finding an atom at position **r** and time t[13].

For a Fickian diffusion process, the self-diffusion function results (see Eq (**3**)) after a double Fourier transform in a scattering function consisting in a Lorentzian of line width given by γ = Dq^2.

$$G_s(r,t) = (4\pi Dt)^{-3/2}e^{-\frac{r^2}{4Dt}} \quad (\mathbf{3})$$

More sophisticated models were developed and found useful such as the jump diffusion model by Singwi and Sjölander for ps-ns internal protein dynamics[14] or the rotation model by Sears for hydration water[15,16,17].

On the neutron backscattering (NBS) instrument IN16B[8,9] at the ILL, Grenoble, France (**Supplemental Figure S1**), a setup commonly used with proteins consists of Si 111 crystals for the analyzers with a Doppler drive for tuning the incoming wavelength (**Supplemental Figure S2A**), thereby giving access to the momentum transfer range ~0.2 $Å^{-1}$ < q < ~2 $Å^{-1}$ and energy transfer range of -30 μeV < $\hbar\omega$ < 30 μeV-corresponding to timescales ranging from a few ps to a few ns and distances of a few Å. In addition, IN16B offers the possibility to perform elastic and inelastic fixed-window scans (E/IFWS)[10], which include data acquisition at

a fixed energy transfer. As the flux is limited when working with neutrons, E/IFWS allows maximization of the flux for one energy transfer, thus reducing the acquisition time needed to obtain a satisfying signal-to-noise ratio. A more recent option is the backscattering and time-of-flight spectrometer (BATS) mode[11], which allows measurement of a wide range of energy transfers, (e.g., -150 μeV < $\hbar\omega$ < 150 μeV), with a higher flux than with the Doppler drive, yet at the cost of a lower energy resolution (**Supplemental Figure S2B**).

An important property of neutron scattering is that the incoherent cross section σ_{inc} has a 40 times higher value for hydrogen than for deuterium and is negligible for other elements commonly found in biological samples. Therefore, the dynamics of proteins in a liquid environment can be studied by using a deuterated buffer, and the powder state allows for the study of either protein internal dynamics with hydrogenated protein powder hydrated with D_2O, or the study of hydration water for perdeuterated protein powder hydrated with H_2O. In the liquid state, neutron backscattering typically allows simultaneously accessing of the center-of-mass self-diffusion of proteins (Fickian-type diffusion) and their internal dynamics. The latter are backbone and side-chain motions usually described by the so-called jump diffusion model or others[3,18]. In hydrogenated protein powders, the protein diffusion is absent and only internal dynamics needs to be modeled. For hydration water, the contributions of translational and rotational motions of water molecules present a different dependence on the momentum transfer **q**, which allows for their distinction in the data analysis process[17].

This paper illustrates the neutron backscattering method with the study of proteins that were found to be able to unfold, aggregate into a canonical form consisting of stacks of β-strands-the so-called cross-β pattern[19,20]-and form elongated fibers. This is the so-called amyloid aggregation, which is extensively studied due to its central role in neurodegenerative disorders such as Alzheimer's or Parkinson's diseases[21,22]. The study of the amyloid proteins is also motivated by the functional role they can play[23,24] or their high potential for the development of novel biomaterials[25]. The physicochemical determinants of the amyloid aggregation remain unclear, and no general theory of amyloid aggregation is available, despite tremendous progress during the past years[21,26].

Amyloid aggregation implies changes in protein structure and stability with time, the study of which naturally implies dynamics, linked to protein conformation stability, protein function, and protein energy landscape[27]. Dynamics is directly linked to the stability of a specific state through the entropic contribution for the fastest motions[28], and protein function can be sustained by motions on various timescales from sub-ps for light-sensitive proteins[29] to ms for domain motions, which can be facilitated by picosecond-nanosecond dynamics[30].

Two examples of using neutron backscattering spectroscopy to study amyloid proteins will be presented, one in the liquid state to study protein dynamics and one in the hydrated powder state to study hydration water dynamics. The first example concerns the aggregation of lysozyme into μm sized spheres (called particulates) followed in real time[5], and the second a comparison of water dynamics in native and aggregated states of the human protein tau[31].

Lysozyme is an enzyme involved in immune defense and is composed of 129 amino acid residues. Lysozyme can form particulates in deuterated buffer at pD of 10.5 and at a temperature of 90 °C. With neutron scattering, we

showed that the time evolution of the center-of-mass diffusion coefficient of lysozyme follows the single exponential kinetics of thioflavin T fluorescence (a fluorescent probe used to monitor the formation of amyloid cross-β patterns[32]), indicating that the formation particulate superstructures and cross-β patterns occur in a single step with the same rate. Moreover, the internal dynamics remained constant throughout the aggregation process, which can be explained either by a fast conformational change that cannot be observed on NBS instruments, or by the absence of significant change in protein internal energy upon aggregation.

The human protein tau is an intrinsically disordered protein (IDP) consisting of 441 amino acids for the so-called 2N4R isoform, which is notably involved in Alzheimer's disease[33]. Using neutron backscattering on powders of perdeuterated protein tau, we showed that hydration water dynamics is increased in the fiber state, with a higher population of water molecules undergoing translational motions. The result suggests that an increase in hydration water entropy might drive the amyloid fibrillation of tau.

Protocol

1. Prepare the deuterated buffer for proteins in the liquid state

1. Dissolve all components of the buffer in pure D_2O.
2. If the pH electrode was calibrated in H_2O, adjust the pD according to the formula pD = pH + 0.4 using NaOD or DCl[34].

   NOTE: The use of D_2O instead of H_2O might affect protein solubility and the buffer conditions might need to be adapted, (e.g., by a slight change in salt concentration).

2. Prepare the H_2O-hydrated powders of perdeuterated protein

1. Prepare the sample holder.
   1. Thoroughly clean a flat aluminum sample holder with its indium wire seal and screws with water and ethanol and let it dry.

      NOTE: A flat sample holder is used such that the powder can be homogenously distributed over the surface. The amount of powder should be sufficient such that it can be maintained between the walls and does not fall when the sample holder is placed vertically.
   2. Weigh the different parts of the sample holder-bottom, lid, and indium wire-separately on a precision balance.
   3. Place the 1 mm indium wire seal in the groove of the bottom part of the sample holder, leaving a small overlap where the two ends join (**Figure 2A**).
   4. Place an appropriate amount of lyophilized protein (typically ~100 mg of protein) such that it fills the inner surface of the bottom part of the sample holder.
2. Hydrate the protein powder.
   1. Place the sample holder in a desiccator with a Petri dish containing P_2O_5 powder for 24 h to completely dry the protein powder[35] (**Figure 2B**). Weigh the dry bottom part of the sample holder containing the indium seal and the dry powder to obtain m_{dry}.

      CAUTION: P_2O_5 powder is very corrosive.

2. Remove the P_2O_5 from the desiccator and put a Petri dish with D_2O inside. Control the mass of the powder regularly to check the hydration level h = m_{hyd} / m_{dry} where m_{hyd} and m_{dry} are the mass of the hydrated powder and dry powder, respectively.
   NOTE: For highly hydrophobic proteins such as insulin, it might be necessary to increase the temperature inside the desiccator to get a higher vapor pressure and reach the desired hydration level h.
3. Repeat steps 2.2.1 and 2.2.2 at least three times to properly convert all exchangeable hydrogens to deuterons.
   NOTE: Alternatively, cycles of freeze-drying and dissolution in pure D_2O might be used for better H/D exchange provided that the protein is not affected by it.
4. Hydrate the powder to slightly above the desired level, let the bottom part of the sample holder with the indium wire and hydrated powder remain on the precision balance, and wait for the mass to decrease slowly to the desired value to get the target h (typically 0.2-0.4 if a medium sized globular protein is to be covered by one complete hydration layer).
5. Quickly put the lid on the bottom part and close the sample holder first with four screws to stop the vapor exchange (**Supplemental Figure S3A**).
6. Place and tighten all remaining screws until no gap is visible between the bottom part and the lid (**Supplemental Figure S3B**).
7. Weigh the sealed sample holder to check for any potential hydration loss via leaks after the neutron experiment.

3. Perform the incoherent neutron scattering experiment

1. Discuss and double-check the configuration of the instrument needed for the experiment with the local contact some weeks before the assigned beamtime.
2. Prepare the liquid state sample.
   1. Dissolve the protein in the deuterated buffer.
   2. Determine the appropriate volume of liquid to be put in the sample holder using water (ensure there is no overflow when the sample holder is closed; **Figure 2C**).
      NOTE: The following steps (3.3 and 3.4) describe an experiment conducted on the NBS spectrometer IN16B at the ILL[8,9], using a cryofurnace as a sample environment. The instrument control system will change from one instrument to the other, but the working principles remain the same.
3. Insert the sample.
   1. Thoroughly dry the sample stick (**Figure 2D**), and remove the previous sample, if any, after checking that the ionizing radiation dose is lower than 100 µSv/h before handling any material (at the ILL).
   2. Place the sample, check for proper centering relative to the beam center (**Supplemental Figure S4**), and insert the sample stick in the cryofurnace (**Figure 2D**). Turn on the vacuum pump to reach less than 10^{-3} bar, and flush out the air inside the cryofurnace by repeating the following three times: fill the cryofurnace with helium gas until atmospheric pressure is reached, and remove the gas again using the vacuum pump.

NOTE: In case of a flat sample holder, the sample holder must be oriented at a 45° angle relative to the incoming beam. The useful momentum transfer range could be reduced due to absorption and scattering by the cell. A strong neutron absorber such as cadmium can be used to mask certain parts of the sample holder (e.g., screws, thick parts).

3. Introduce some helium gas in the cryofurnace such that the pressure is ~0.05 bar.

4. Acquire data (e.g., using NOMAD on IN16B at the ILL, it is assumed that the user prefers a temperature of 200 K before acquiring a quasielastic neutron spectrum (QENS) spectrum, then E/IFWS during a temperature ramp to 310 K at 0.5 K per min and finally a QENS at 310 K).

    1. Using **NOMAD**, in the **execution** tab, drag and drop a **FurnaceCryostat** controller in the **Launch Pad**. Set the **temperature** to **200 K**. Use the **fast** mode and a **timeout** of **30 min** such that the temperature has time to stabilize. Click on the **rotating arrows** icon to run it in the background such that data can be acquired during the temperature decrease.

    2. Drag and drop the **IN16DopplerSettings** controller, set the **speed profile** to **Accurate velocity** set by **Max ΔE**, a value of **0.00 μeV** and **128 channels** to obtain an EFWS configuration.

    3. Drag and drop a **Count** controller, fill the **Subtitle** field with a name that allows easy identification of the data, and set **60 repetitions** of **30 s scans** (**Supplemental Figure S5A**).

    4. Drag and drop an **IN16DopplerSettings** controller, set the **speed profile** to **Sine** set by **Speed** with a value of **4.5 m/s** and **2,048 channels** to obtain a QENS configuration.

    5. Drag and drop a **Count** controller with **4 repetitions of 30 min scans** (**Supplemental Figure S5B**).

    6. For the temperature ramp, drag and drop a **FurnaceCryostat** controller, set the **temperature** to **310 K**, set **Ramp** to **SetPoint** with **Δ = 0.05 K** and **6 s**. Use a **time out** of **220 min** (**Supplemental Figure S6A**).

    7. Use a **for loop** with **65 repetitions**. Inside, insert an **IN16DopplerSettings** controller as in step 3.4.2, followed by a single count of **30 s**. Subsequently, insert **IN16DopplerSettings**, as described previously but using an **energy offset** of **1.5 μeV** and **1,024 channels** followed by a single count of **3 min** (**Supplemental Figure S6B**).

    8. To acquire the last QENS at 310 K, drag and drop **IN16DopplerSettings** and **Count** controllers configured as described in steps 3.4.4 and 3.4.5, respectively.

    9. Press the **start** button (right triangle on the bottom of the window) to run the script.

    NOTE: Every experiment will require the acquisition of calibration data; that is, the empty cell for subtraction or absorption corrections, the buffer alone at the different temperatures used to model the background, and a measurement of vanadium (or equivalently, the sample at a temperature of 10 K or lower) to obtain the resolution function of the instrument.

4. Data analysis - QENS

1. Import the dataset using the 'IN16B_QENS.process()' method in the Python software nPDyn v3.x[36]

```
>>>> from nPDyn.dataParsers import IN16B_QENS
>>> sample = IN16B_QENS(
...<path to data files>
... [detGroup=<integer or detector grouping file in XML
...format>]
... ).process()
>>> sample = sample.get_q_range(0.3, 1.8)
```

2. Perform data corrections (optional) with the following commands (see the documentation of nPDyn for more information, **Figure 3**):

```
#it is assumed that data for empty cell, vanadium, and buffer
# were imported already in dataset called 'empty_cell', 'vanadium',
# and 'buffer', respectively.
# for empty cell subtraction with a scaling factor
# (errors are propagated automatically)
>>> sample = sample - 0.95 * empty_cell
# for correction using Paalman-Ping coefficient
# (mutually exclusive with the example above)
>>> sample = sample.absorptionCorrection(empty_cell)
# for normalization
>>> sample = sample.normalize(vanadium)
# for binning along observable axis
# observable is the aggregation time here
>>> sample = sample.bin(3, axis=0)
```

3. Fit the calibration data. The dataset-samples, empty cell, deuterated buffer (if needed), and vanadium-can be fitted using built-in models or a user-defined model (see nPDyn documentation):

```
>>> from nPDyn.models.builtins import (
... modelPVoigt,
... modelWater,
...modelCalibratedD2O,
... )
# builtin models use a column vector of the momentum
# transfer q values
>>> q = vanadium.q[:, None]
# the vanadium is fitted using a pseudo-Voigt profile
>>> vanadium.fit(modelPVoigt(q))
```

4. Use the built-in model for hydration water called 'modelWater'. This model reads as shown by Eq (**4**)[17]

$$S(\mathbf{q},\omega) = R(\mathbf{q},\omega) \otimes \left[(a_r j_0^2(qd) + a_0)\delta(\omega) + \sum_1^N (2l+1) j_l^2(qd) a_r \mathcal{L}_{l(l+1)\gamma_r} + a_t \mathcal{L}_{\gamma_t} \right] + b(q) \quad (\mathbf{4})$$

Where a_0, a_r, and a_t are scalars accounting for the relative contribution of elastic signal, rotational motions, and translational motions, respectively; $j_1(qd)$ is the l^{th} order spherical Bessel function, with q being the momentum transfer; d the O-H distance in the water molecule; δ(ω) is the Dirac delta, which is multiplied by the EISF here; N is the highest order of the spherical Bessel function used (typically ~5); $\mathcal{L}_{l(l+1)\gamma_r}$ and $\mathcal{L}_{\gamma_t}$ are the Lorentzian rotational and translational motions, respectively; b(q) is a flat background term. The spherical Bessel functions give the relative contribution of each angular momentum state of the water molecules, and the number N is determined based on the momentum transfer q-range. In the case of a typical NBS spectrometer, the terms up to N = 4 almost entirely explain the signal (**Supplemental Figure S7**).

 # here, equation 2 is used for hydration water

 # convolution with resolution function and addition of

 # D2O background is done automatically with the

 # provided arguments

>>> sample.fit(modelWater(q),

... res=vanadium,

... bkgd=buffer,

... volume_fraction_bkgd=0.95

...)

NOTE: The contributions of rotational and translational motions should be convoluted to be perfectly rigorous. The success of an additive model is to be attributed to the presence of distinct populations of water on the protein surface and the limited energy range accessible.

5. Use the following to plot the data (**Figure 4**):

>>> from nPDyn.plot import plot

>>> plot(sample)

5. Data analysis - temperature ramp, elastic fixed-window scans (EFWS)

1. Use a procedure similar to section 4 to normalize the temperature ramp data by the signal at the lowest temperature (typically 10 K):

>>> from nPDyn.dataParsers import IN16B_FWS

>>> sample = IN16B_FWS(

... <path to data files>,

... detGroup=[detGroup=<integer or detector grouping file in XML format>]

...).process()

 # normalization with the 5 first points on the observable

 # axis, which correspond to the temperature

>>> sample /= sample[:5].mean(0)

 # the momentum transfer q range used here is smaller

 # as the model used is valid for low q only

>>> sample = sample.get_q_range(0.2, 0.8)

2. Use a simple Gaussian model to start, the width of which is given by the so-called mean squared displacement (MSD). Build and fit the model using the following commands:

>>> import numpy as np

>>> from nPDyn.models import Parameters, Model, Component

 # a is a scaling factor

>>> params = Parameters(

... a={'value': 1, 'bounds': (0, np.inf)},

... msd={'value': 1, 'bounds': (0, np.inf)}

...)

>>> model = Model(params)

>>> model.addComponent(Component(

… 'gaussian',

*… lambda x, a, msd: a * np.exp(-x ** 2 * msd / 6)*

…))

>>> sample.fit(model, x=sample.q[:, None])

>>> plot(sample)

NOTE: The Gaussian approximation always holds for q^2MSD << 1, but wider momentum transfer range can be used for relative comparison between samples. More sophisticated models, which go beyond the Gaussian approximation, have been developed[37,38,39].

6. Data analysis - elastic and inelastic fixed-window scans (E/IFWS)

1. Similar to step 4, import the dataset but using the 'IN16B_FWS' class:

>>> from nPDyn.dataParsers import IN16B_FWS

>>> sample = IN16B_FWS(

...<path to data files>

... [detGroup=<integer or detector grouping file in XML format>]

...).process()

>>> sample = sample.get_q_range(0.3, 1.8)

2. Fit the calibration data and sample data.

    1. Analyze the E/IFWS data using a generalized MSD[40] or by considering them as coarse-QENS spectra (having only a few data points on the energy axis). When E/IFWS is viewed as coarse-QENS, models used for QENS are used to fit the whole E/IFWS dataset at once (global fit of energy transfers and momentum transfers).

        NOTE: The latter solution-using models for QENS on E/IFWS data-is used here where the momentum transfer dependence of center-of-mass diffusion and protein internal dynamics are imposed.

    2. Model protein dynamics in liquids using the following Eq (**5**) ('modelProteinJumpDiff' in nPDyn):

$$S(\mathbf{q},\omega) = R(\mathbf{q},\omega) \otimes \beta(\mathbf{q})\left[a_0(\mathbf{q})\mathcal{L}_\gamma(\mathbf{q},\omega) + \left(1 - a_0(\mathbf{q})\right)\mathcal{L}_{\gamma+\Gamma}(\mathbf{q},\omega)\right] + \beta_{D_2O} R(q,\omega) \otimes \mathcal{L}_{D_2O} \quad (\mathbf{5})$$

        Where R(**q**,ω) is the resolution function; β a scalar independent for each momentum transfer q; a_0 is the elastic incoherent structure factor (EISF); $\mathcal{L}_\gamma$ a Lorentzian accounting for center-of-mass diffusion with a width given by Eq (**6**); $\mathcal{L}_{\gamma+\Gamma}$ is a Lorentzian that includes center-of-mass diffusion and a contribution following the jump-diffusion model[14] accounting for internal dynamics (Eq (**7**); $\beta_{D_2O}\mathcal{L}_{D_2O}$ being the fitted signal from D_2O rescaled by its volume fraction in the sample.

$$\gamma = D_S q^2 \quad (\mathbf{6})$$

D_S being the self-diffusion coefficient.

$$\Gamma = D_i q^2/(1 + D_i q^2 \tau) \quad (\mathbf{7})$$

D_i being the apparent diffusion coefficient for internal dynamics and τ a relaxation time for diffusive motions.

>>> from nPDyn.models.builtins import (

... modelPVoigt,

... modelProteinJumpDiff,

...modelCalibratedD2O,

...)

 # builtin models use a column vector of the momentum

 # transfer q values

>>> q = vanadium.q[:, None]

 # the vanadium is fitted using a pseudo-Voigt profile

>>> vanadium.fit(modelPVoigt(q))

 # for pure D2O, a model with calibrated linewidth

 # for different temperatures is included in nPDyn

>>> buffer.fit(modelCalibratedD2O(q, temp=363))

 # here, equation 3 is used for liquid samples

 # convolution with resolution function and addition of

 # D2O background is done automatically with the# provided arguments

>>> sample.fit(modelProteinJumpDiff(q),

... res=vanadium,

... bkgd=buffer,

... volume_fraction_bkgd=0.95

...)

3. Plot the fitted data using:

    >>> from nPDyn.plot import plot

    >>> plot(sample)

Representative Results

The aggregation of lysozyme into particulates was performed at 90 °C with a protein concentration of 50 mg/mL in a deuterated buffer (0.1 M NaCl at pD 10.5). The formation of particulates is triggered by the temperature increase to 90 °C and occurs within 6 h (**Supplemental Figure S8**). The data acquisition was performed on IN16B, as described in the protocol above (data are permanently curated by the ILL and accessible at http://dx.doi.org/10.5291/ILL-DATA.8-04-811).

A QENS spectrum was acquired at 7 °C to fully characterize the initial state. Subsequently, the temperature was increased to 90 °C (typically takes ~30 min on IN16B, **Supplemental Figure S9**) to trigger the aggregation process. The kinetics can be followed using a sliding average of QENS spectra, allowing access to the full range of energy transfer, yet with a limited resolution in time. The time resolution can be improved to ~1 min using EFWS and to ~20 min using E/IFWS at four energy transfer values[5].

In the example presented, we explored energy transfers of 0, 0.6, 1.5, and 3 μeV. The E/IFWS scans are acquired continuously during the aggregation process, and a QENS spectrum was acquired for the final state at 90 °C. The E/IFWS data were corrected for absorption using the E/IFWS of the empty cell and normalized using the vanadium data.

For the lysozyme E/IFWS, we observe an increase of the signal in time at low momentum transfer and low energy transfer, while the signal at high energy transfer and low momentum transfer decreases (**Supplemental Figure 10**). This qualitative observation indicates the formation of larger objects, diffusing more slowly and confirming that the aggregation process took place. The analysis, according to Eq (4), results in an initial center-of-mass diffusion coefficient of 15 $Å^2$/ns, in agreement with the presence of small protein clusters (supported by dynamic light scattering and HYDROPRO calculations[5,41]), which then exponentially decreases over time (**Figure 5**). The apparent diffusion coefficient for internal dynamics remains constant throughout the aggregation process. Hence, the formation of lysozyme particulates appears to occur in a single aggregation phase. The absence of change in internal protein dynamics suggests that either the conversion to cross-β and the possible associated change in energy are too fast or that other driving effects, such as an increase in solvent entropy, might be fully dominating within the energy range probed.

The study of hydration water dynamics around monomers and fibers of tau was performed on SPHERES at the Maier-Leibnitz Zentrum (MLZ) in Garching, Germany, using the protocol described above for powder samples. Approximately 100 mg of deuterated tau protein powder, hydrated to 0.4 g of H_2O per g of protein, was used. EFWS were acquired during a temperature ramp and QENS spectra at constant temperature. The EFWS were recorded starting at 20 K and increasing the temperature to 300 K at a rate of 0.2 K/min while continuously acquiring data during 5 min scans.

The QENS spectra were recorded at 20 and at 280 K. The EFWS data were fitted using a simple Gaussian over the momentum transfer q range 0.2 $Å^{-1}$ < q < 0.8 $Å^{-1}$ to extract the MSD (**Supplemental Figure S11A**). The MSD values are above the validity limit for the Gaussian model. Hence, it is recommended in this case to explore other models beyond the Gaussian approximation[37,38,39]. At temperatures higher than 220 K, the hydration water around fibers of tau is significantly more mobile than hydration water around tau monomers (**Figure 6**). The fitting of QENS data allows users to obtain the linewidth and relative contribution of elastic,

rotational, and translational motions of hydration water in the sample (**Supplemental Figure S11B**). It appears that the fraction of water molecules undergoing translational motion is increased around fibers, and both translational and rotation diffusion coefficients of water molecules are increased around fibers[17,31]. In contrast, the ps-ns internal dynamics of the protein tau, reflecting backbone and side-chain motions, did not change upon fibrillation.

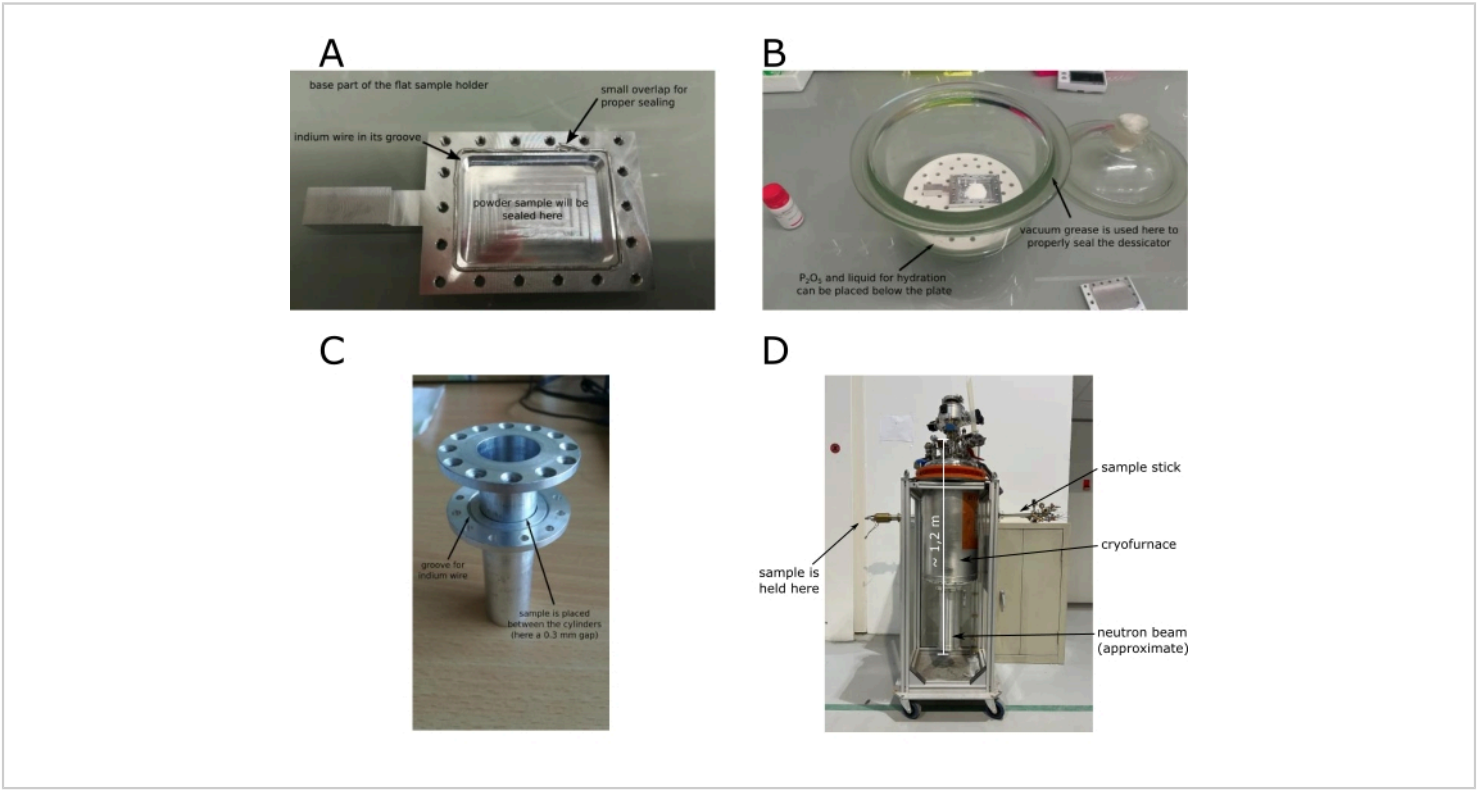

Figure 2: Base of a flat aluminum sample holder. (**A**) The flat aluminum sample holder presents a central part exposed to the neutrons where the protein powder is maintained within a small gap-typically ~0.3 mm-between the base and the lid. An indium wire can be used for sealing as it resists temperature increases up to 90 °C. In case of higher temperatures, a Teflon seal can be used. (**B**) The protein powder is placed in the base of the sample holder with the indium wire in place. The sample holder is placed in a desiccator in presence of either P_2O_5 for drying or H_2O/D_2O for hydration. Vacuum grease is added to avoid any leak between the bottom and the lid of the desiccator. Vacuum can be used with caution to accelerate the drying process. Heating the bottom of the desiccator may be required for highly hydrophobic samples. (**C**) The protein solution is placed between the inner and outer cylinders. Make sure not to pipette too much liquid (there should be no overflow when the sample holder is closed). The indium wire is placed in the circular groove. (**D**) The sample stick (in the background) provides control on the sample height and orientation and can include different controllers and detectors for sample environments (temperature, pressure). The sample stick is inserted from the top of the cryofurnace (front), which provides control for the temperature during the experiment. During the experiment, the neutron beam usually hits the bottom

of the cryofurnace, as indicated by the white rectangle (the size of the beam depends on the instrument configuration).

Please click here to view a larger version of this figure.

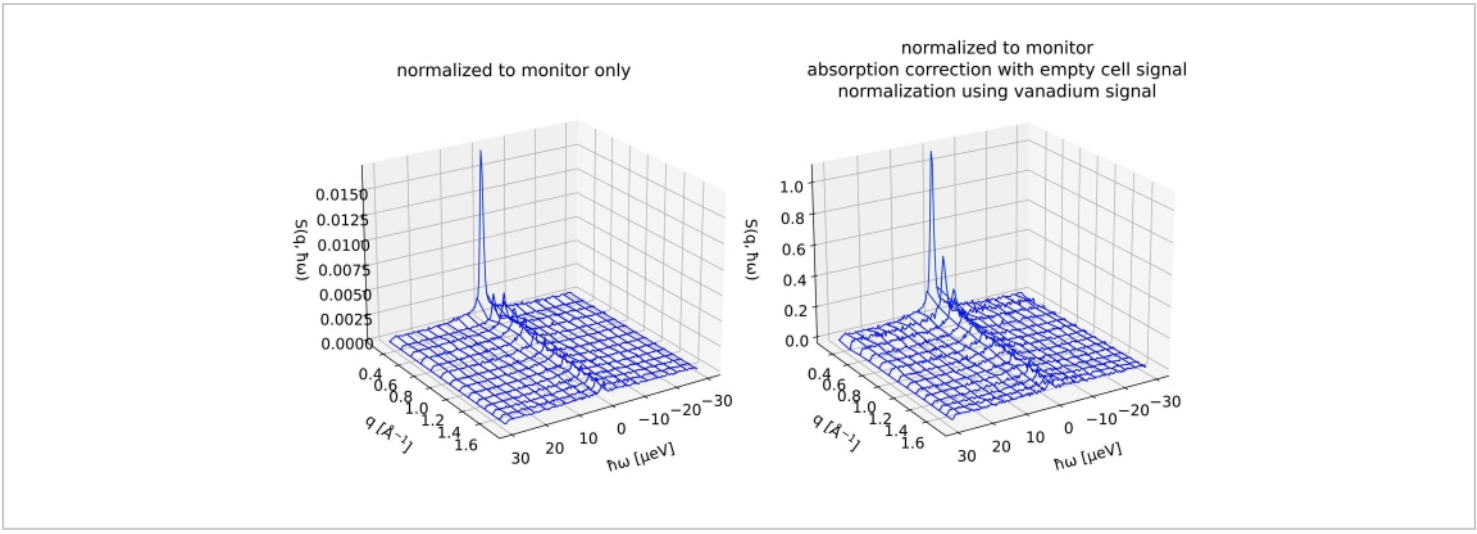

Figure 3: Data corrections and normalization may improve the fit. The data were imported using nPDyn, as described in the protocol. **Left**, the dataset was normalized using the data of the monitor only. **Right**, the signal of the empty can was used along with the Paalman-Ping coefficients[43] to correct for neutron absorption from the sample holder. Subsequently, the fitted model for the vanadium signal was integrated independently for each momentum transfer q, and the result was used to normalize the sample dataset. In both plots, S(q,ω) denotes the scattering signal, q is the momentum transfer, and $\hbar\omega$ is the energy transfer. Please click here to view a larger version of this figure.

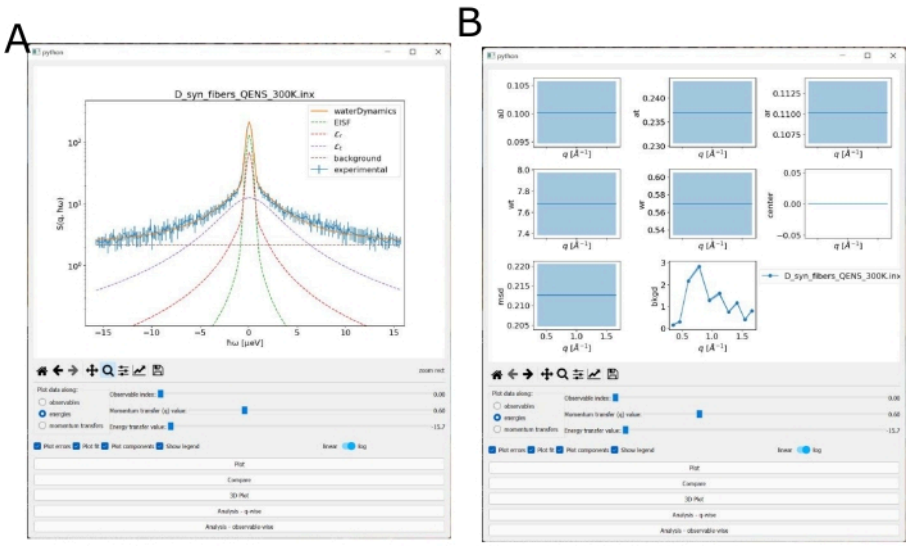

Figure 4: Plotting window generated by nPDyn showing the result of the fit. The QENS data were fitted using nPDyn, as described in the protocol. The plotting window allows users to plot the data along different axes-observable (time, temperature or pressure), momentum transfer q or energy transfer-and selectors are available to navigate along the other axes. Different types of plot are available, with the simple '**Plot**' presented in (**A**) and '**Analysis - q-wise**' in (**B**). The '**Plot**' button shows the different datasets in separate subplots, the '**Compare**' button shows the datasets in the same plot, the '**3D plot**' shows the datasets in different 3D subplots similar to s, '**Analysis - q-wise**' button shows the fitted parameters as the function of momentum transfer q and '**Analysis - observable-wise**' shows the fitted parameters as the function of observable (time, temperature or pressure). Abbreviation: QENS = quasielastic neutron scattering. Please click here to view a larger version of this figure.

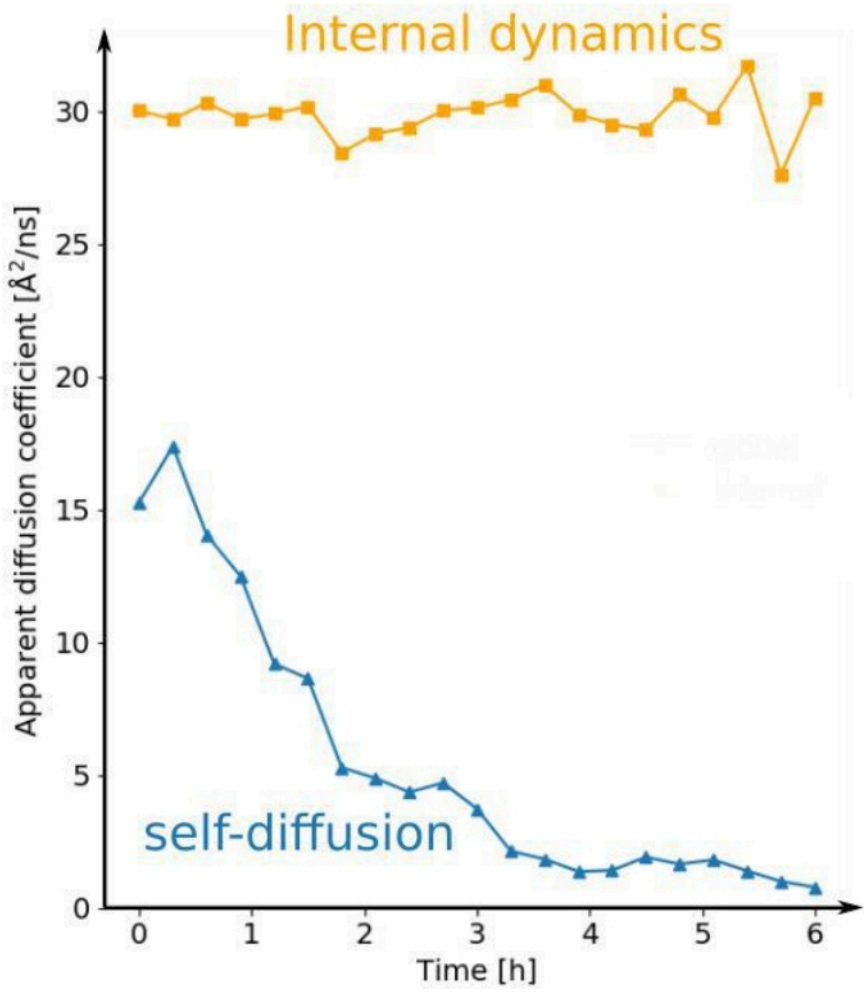

Figure 5: Lysozyme aggregation occurs in a one-step process with constant internal dynamics. The lysozyme was dissolved in the aggregation buffer (described elsewhere[5]), and E/IFWS was acquired throughout aggregation, which was triggered by increasing the temperature to 90 °C. After absorption correction with an empty cell and normalization using the vanadium signal, the data were analyzed using the jump diffusion model as described in the protocol. The fitted center-of-mass self-diffusion coefficient is plotted as a function of time (blue triangles) along with the apparent diffusion coefficient for internal dynamics (orange squares). This figure is from [5]. Abbreviation: E/IFWS = elastic and inelastic fixed-window scans. Please click here to view a larger version of this figure.

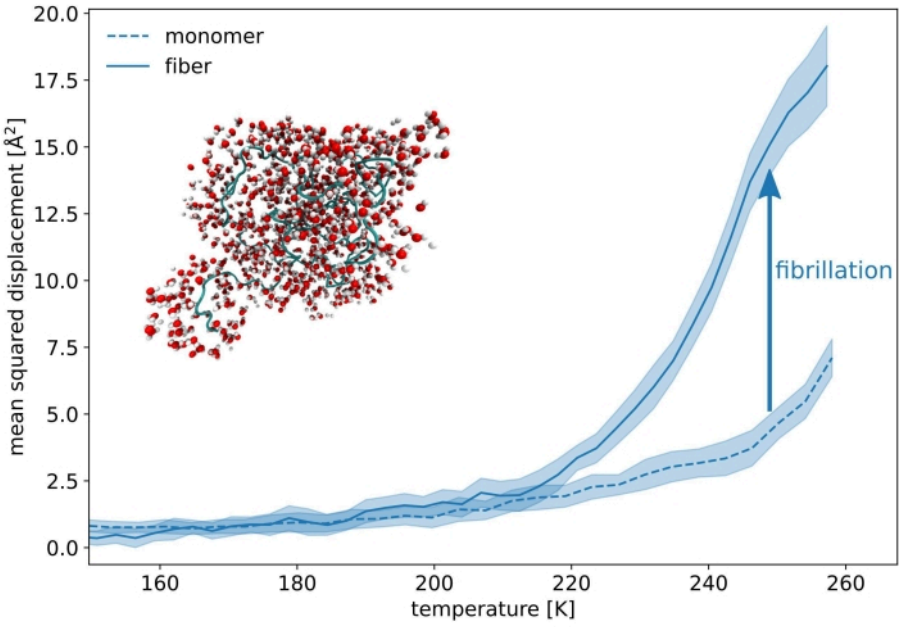

Figure 6: Hydration water dynamics is increased around tau fibers. The H_2O-hydrated powders of deuterated tau fibers and monomers were sealed in a flat aluminum sample holder, and EFWS data were acquired during a temperature ramp from 20 to 300 K. After absorption correction with an empty cell and normalization using the vanadium signal, the data were analyzed using the jump diffusion model as described in the protocol. This image was redrawn using a smaller q range ($0.2 < q < 0.8$ Å^{-1}) from data from [31]. Abbreviation: EFWS = elastic fixed-window scans. Please click here to view a larger version of this figure.

Supplemental Figure S1: Photographs of the instrument IN16B at the ILL. (top) The instrument IN16B as seen from the radiation-controlled zone dedicated to the instrument. The incoming beam travels within the neutron guide to the vacuum chamber, which contains most of the elements of the instrument (PST chopper, analyzers, sample, detectors). **(bottom)** Interior of the vacuum chamber. The PST chopper is visible as are the analyzers surrounding the cryofurnace containing the sample. The detectors are located behind the cryofurnace. Courtesy of Laurent Thion, ecliptique. Abbreviation: PST = phase space transformation. Please click here to download this File.

Supplemental Figure S2: Sketch of IN16B in classical (with Doppler drive) and BATS modes. (**A**) The neutron beam is partly monochromatized by the velocity selector. Subsequently, the background and PST choppers will produce a neutron pulse, from which an energy profile will be selected by the Doppler monochromator (E/IFWS or QENS mode). The neutrons are then scattered by the sample, and a single energy is reflected toward the detectors by the analyzers. Courtesy of the ILL. (**B**) The BATS choppers are used to define a single neutron pulse with a defined energy range. The neutron beam is partly monochromatized by the velocity selector. Subsequently, the background chopper will

remove unwanted neutrons that do not belong to the selected pulse. The neutrons are then scattered by the sample, and a single energy is reflected toward the detectors by the analyzers. Courtesy of the ILL. Abbreviations: BATS = backscattering and time-of-flight spectrometer; PST = phase space transformation; E/IFWS = elastic and inelastic fixed-window scans; QENS = quasielastic neutron scattering; PG = pyrolytic graphite. Please click here to download this File.

Supplemental Figure S3: The sample holder is closed quickly after the powder has reached the desired hydration and sealed. (**A**) The flat sample holder is quickly closed using four screws. A small gap will remain due to the indium wire. The other screws are then added, and the sample holder is sealed slowly by gently tightening each screw several times to allow the indium to relax. (**B**) The flat sample holder is properly sealed when no gap is visible anymore between the holder base and the lid. Please click here to download this File.

Supplemental Figure S4: The sample holder is centered with respect to the neutron beam. A cylindrical sample holder has been placed on the sample stick. The position of the sample holder is checked such that the beam hits the bottom part of the holder. Please click here to download this File.

Supplemental Figure S5: Acquisition of EFWS followed by QENS on IN16B with NOMAD. (**A**) The relevant controllers are dragged and dropped into the **Launch Pad** as explained in the protocol (steps 3.4.1 to 3.4.3). It might be necessary to click on the lock (green icon at the top-right corner - vertical pane) to obtain control on the interface. (**B**) The relevant controllers are dragged and dropped into the **Launch Pad** as explained in the protocol (steps 3.4.4 to 3.4.5). Here, the last two controllers are named **IN16DopplerSettings** and **Count**. Abbreviations: QENS = quasielastic neutron scattering, EFWS = elastic fixed-window scans. Please click here to download this File.

Supplemental Figure S6: Setting up a temperature ramp and E/IFWS on IN16B with NOMAD. (**A**) The **FurnaceCryostat** controller is added in the **Launch Pad** and configured as explained in the protocol (step 3.4.6). (**B**) The **For loop** controller is added in the **Launch Pad** and relevant controllers are inserted into it and configured as explained in the protocol (step 3.4.7). Abbreviation: E/IFWS = elastic and inelastic fixed-window scans. Please click here to download this File.

Supplemental Figure S7: The first five spherical Bessel functions explain most of the rotational contribution of hydration water. The first eight spherical Bessel functions are plotted using a value d = 0.98 Å and values of momentum transfer q from 0 to 3 Å (solid colored lines). The momentum transfer range of 0.3 Å < q < 1.8 Å is delimited by the blue dotted lines. Please click here to download this File.

Supplemental Figure S8: Lysozyme reproducibly forms particulates. Lysozyme was dissolved in the aggregation buffer (prepared as described in the protocol, step 1), and ThT was added to a final concentration of 2 µM to monitor the formation of cross-β structure using fluorescence. The plot represents the average of three independent measurements, and the error bars are the standard deviation. The inset shows a fluorescence microscopy photograph of the particulates formed after 6 h of aggregation. Scale bar = 20 µm. This figure is from [5]. Abbreviation: ThT = thioflavin T. Please click here to download this File.

Supplemental Figure S9: Fast temperature ramp as available on IN16B. In the **fast** mode on IN16B, the

temperature can be increased from 280 K to 363 K in approximately 30 min. This figure is from [5]. Please click here to download this File.

Supplemental Figure S10: E/IFWS data on lysozyme during aggregation into particulates. The lysozyme was dissolved in the aggregation buffer (described elsewhere[5]), and E/IFWS was acquired throughout aggregation, which was triggered by increasing the temperature to 90 °C. The data-after absorption correction with an empty cell and normalization using the signal of vanadium-are plotted against momentum transfer q and time for the different energy transfer measured, 0 μeV (upper left), 0.6 μeV (upper right), 1.5 μeV (lower left), and 3 μeV (lower right). For each subplot, the vertical axis corresponds to the scattering signal S(q, ΔE), plotted against the experimental time in hours and the momentum transfer q. This figure is from [5]. Abbreviation: E/IFWS = elastic and inelastic fixed-window scans. Please click here to download this File.

Supplemental Figure S11: Fitting of hydration water data of tau. (**A**) Fit of the EFWS data using a Gaussian. The H_2O-hydrated powder of deuterated tau monomers was sealed in a flat aluminum sample holder, and EFWS were acquired during a temperature ramp from 20 to 300 K. The experimental data (elastic signal S(q, 0) on vertical axis-blue line with error bars) are plotted for the momentum transfer q range $0.2 < q < 0.6$ Å^{-1} along with the fitted Gaussian used to extract the MSD. (**B**) Translational and rotational motions of hydration water obtained from QENS fitting. The H_2O-hydrated powders of deuterated tau fibers (**left**) and monomers (**right**) were sealed in a flat aluminum sample holder, and QENS data were acquired at 280 K. The experimental data (intensity S(q,ω) as the function of energy transfer) for fibers (blue triangles) and monomers (green dots) are plotted along with the fitted model (black solid line) and its components, background (blue), resolution function (green), rotations (red), and translations (cyan) for the momentum transfer q = 0.783 Å^{-1}. This figure is from [31]. Abbreviations: QENS = quasielastic neutron scattering, EFWS = elastic fixed-window scans; MSD = mean squared displacement. Please click here to download this File.

Discussion

Neutron spectroscopy is the only method that allows probing the ensemble-averaged ps-ns dynamics of protein samples regardless of the size of the protein or the complexity of the solution when deuteration is used[6]. Specifically, by probing self-diffusion of protein assemblies in solution, the hydrodynamic size of such assemblies can be unambiguously determined. Nonetheless, the method is commonly limited by the low neutron flux, which implies long acquisition times and the requirement of high amounts of sample (typically 100 mg of protein) to obtain a good signal-to-noise ratio within the allocated beam time.

Sample preparation (protocol steps 1 and 2). For liquid-state samples, the minimum concentration that can be used is ~50 mg/mL (lower concentrations can be used at the cost of extended acquisition times). High protein concentration is associated with faster fibrillation rates, which helps with fitting the measurement in the allocated beam time but can affect the aggregation pathway too[44]. Hence, thorough sample characterization with complementary methods, such as atomic force or electron microscopy, is necessary.

The material of the sample holder is also a point to be addressed when preparing the samples as aluminum alloys are subject to corrosion[45]. A typical aluminum alloy that presents good resistance to corrosion and has low neutron absorbance is the European Norm (EN) AW-6060 [AlMgSi]

made of 98%-98.75% Al, 0.1% Ti, 0.15% Zn, 0.05% Cr, 0.35%-0.6% Mg, 0.1% Mn, 0.1% Cu, 0.1%-0.3% Fe, and 0.3%-0.6% Si. Corrosion can be minimized for instance by reducing the time in the sample holder or using a protective coating (which can add to the background signal) such as nickel or gold.

For powder samples of hydrogenated proteins, the freeze-drying procedure was shown to be efficiently completed with a step in a desiccator in the presence of P_2O_5 powder to remove as much residual light water as possible[35]. For powder samples, it is also advised to characterize (using atomic force microscopy and X-ray powder diffraction) the powder in its final, hydrated state and assess the effect of deuteration, freeze-drying, and vapor diffusion on both monomer and fiber states. In particular, freeze-drying can break the fibers, resulting in shortened segments, without affecting the morphology. Moreover, it has been observed by X-ray power diffraction that slow cooling, instead of flash cooling in liquid nitrogen, could induce the presence of amyloid-like structures (unpublished result).

Data collection (protocol step 3). It is advised to plan the data collection with the local contact prior to the experiment (even if it has been discussed during the proposal writing process). The data collection plan is subject to changes after the first scans, depending on the signal-to-noise ratio obtained. For time-resolved experiments in particular, the use of E/IFWS allows for fast data collection-30 s to 1 min for the elastic line, 4-5 min for a data point at 3 μeV[5]-but the range of accessible energy transfers is inherently limited. Alternatively, a sliding average of QENS data can be used[46]. To this end, the new backscattering and time-of-flight spectroscopy (BATS) option on IN16B offers a higher flux than the classical IN16B with a range of energy of ±150 μeV (or higher depending on the configuration used) at the cost of lower resolution in energy[11]. Therefore, the BATS option is recommended for time-resolved studies, especially for processes such as the amyloid aggregation, which takes place over several hours.

Data analysis (protocol steps 4, 5, and 6). The scattering function $S(q,\omega)$ includes all types of motions in the sample, and the models described in the above protocol are approximations. In particular, for IDP in the liquid state, the large-scale motions of the disordered chain can occur over the same length and timescale as the center-of-mass diffusion of the entire protein. Hence, the user should keep in mind that the separation of center-of-mass diffusion and protein internal dynamics is not always straightforward. The fitting procedure can benefit from information on center-of-mass diffusion obtained via complementary methods, such that this parameter can be fixed (keeping in mind that other methods can provide a collective diffusion coefficient associated with different time and length scales) to obtain a more robust result for internal dynamics.

In addition to neutron scattering, the dynamics of a molecular system can be characterized by nuclear magnetic resonance (NMR), which provides local information on isotope-labeled proteins and on a wide range of timescales[47,48,49]. The method has been used successfully to study amyloid systems[48,50,51,52,53] but does not allow users to simply study hydration water or follow the amyloid aggregation process in real time due to the inherent limitation on the protein size. Recent developments in electron paramagnetic resonance spectroscopy (EPR) and the EPR-derived method Overhauser dynamic nuclear polarization (ODNP) offer a good perspective when combined with neutron scattering. Indeed, though site-directed spin labeling (SDSL), EPR

and ODNP can probe protein[54] and hydration dynamics[55], respectively, on the ps-ns timescale around the introduced spin label.

These methods were used to study the aggregation of the tau[56,57] protein and will offer great complementarity with neutron scattering that can obtain similar information, but averaged over the entire sample. Moreover, infrared spectroscopy can provide dynamical information for high-energy motions associated with specific structural patterns, but the complexity of the protein environment (buffer used) can affect data interpretation[58,59]. The neutron backscattering techniques provide a unique and complementary view on protein and hydration water dynamics on the ps-ns timescale along with results from the aforementioned methods. They do not require specific labeling of the sample, the signal quality is not sensitive to the size of the protein, and measurements can be done *in vivo* or in highly complex, deuterated environments such as deuterated bacterial lysate[3,6,7]. As this method provides an ensemble-averaged result, it is well complemented by molecular dynamics simulations to obtain atomic-detail information on the system under study. The simulations can be easily validated by a direct comparison between the experimental dataset and the theoretical QENS spectra computed from the simulation trajectory using software such as *mdanse*[60].

Regarding amyloid systems, neutron backscattering has proven useful to characterize the ps-ns protein and water dynamics for various systems and conditions[5,31,61,62,63,64]. In particular, neutron backscattering was used to reveal the correlation between the proportion of the protein sequence involved in the cross-β structure and the amplitude of the water entropy gain upon fibrillation (unpublished results). Furthermore, development of sample environments allow the simultaneous acquisition of neutron spectra and either dielectric relaxation data[65] or Raman scattering data[66]. Moreover, diffraction detectors are present on IN16B to obtain structural data along with dynamical data. Additionally, the incoming neutron flux is expected to be improved for the BATS mode of IN16B in the near future, thanks to the use of the so-called variable focusing guide, the geometry of which can be adapted on demand to the instrumental setup used. Pushing the development of sophisticated sample environment and instrumentation further would allow for even more complex experiments in the future, possibly delivering further dynamical and structural information at the same time.

Disclosures

The authors have no conflicts of interest to disclose.

Acknowledgments

The authors are grateful to Michaela Zamponi at the Jülich Centre for Neutron Science at the Heinz Maier-Leibnitz Zentrum, Garching, Germany, for part of the neutron scattering experiments conducted on the instrument SPHERES. This work has benefited from the activities of the Deuteration Laboratory (DLAB) consortium funded by the European Union under Contracts HPRI-2001-50065 and RII3-CT-2003-505925, and from UK Engineering and Physical Sciences Research Council (EPSRC)-funded activity within the Institut Laue Langevin EMBL DLAB under Grants GR/R99393/01 and EP/C015452/1. Support by the European Commission under the 7th Framework Programme through the Key Action: Strengthening the European Research Area, Research Infrastructures is acknowledged [Contract 226507 (NMI3)]. Kevin Pounot and Christian Beck

thank the Federal Ministry of Education and Research (BMBF, grant number 05K19VTB) for funding of their postdoctoral fellowships.

References

1. Jacrot, B. *Des neutrons pour la science: Histoire de l'Institut Laue-Langevin. Des neutrons pour la science.* EDP Sciences (2021).
2. Mahieu, E., Gabel, F. Biological small-angle neutron scattering: recent results and development. *Acta Crystallographica Section D.* **74** (8), 715-726 (2018).
3. Grimaldo, M., Roosen-Runge, F., Zhang, F., Schreiber, F., Seydel, T. Dynamics of proteins in solution. *Quarterly Reviews of Biophysics.* **52**, e7 (2019).
4. Martel, A. et al. Membrane permeation versus amyloidogenicity: A multitechnique study of islet amyloid polypeptide interaction with model membranes. *Journal of the American Chemical Society.* **139** (1), 137-148 (2017).
5. Pounot, K. et al. Tracking internal and global diffusive dynamics during protein aggregation by high-resolution neutron spectroscopy. *The Journal of Physical Chemistry Letters.* **11** (15), 6299-6304 (2020).
6. Grimaldo, M. et al. Protein short-time diffusion in a naturally crowded environment. *The Journal of Physical Chemistry Letters.* **10** (8), 1709-1715 (2019).
7. Jasnin, M., Stadler, A., Tehei, M., Zaccai, G. Specific cellular water dynamics observed in vivo by neutron scattering and NMR. *Physical Chemistry Chemical Physics.* **12** (35), 10154-10160 (2010).
8. Frick, B. The neutron backscattering spectrometer IN16 at ILL-high energy resolution with high intensity and excellent signal-to-noise ratio. *Neutron News.* **13** (2), 15-22 (2002).
9. Frick, B., Mamontov, E., Eijck, L. van, Seydel, T. Recent backscattering instrument developments at the ILL and SNS. *Zeitschrift für Physikalische Chemie.* **224** (1-2), 33-60 (2010).
10. Frick, B., Combet, J., van Eijck, L. New possibilities with inelastic fixed window scans and linear motor Doppler drives on high resolution neutron backscattering spectrometers. *Nuclear Instruments and Methods in Physics Research Section A: Accelerators, Spectrometers, Detectors and Associated Equipment.* **669**, 7-13 (2012).
11. Appel, M., Frick, B., Magerl, A. A flexible high speed pulse chopper system for an inverted neutron time-of-flight option on backscattering spectrometers. *Scientific Reports.* **8** (1), 13580 (2018).
12. Squires, G. L. *Introduction to the theory of thermal neutron scattering.* Mineola N.Y.: Dover Publications (1996).
13. Bee, M. *Quasielastic neutron scattering.* http://inis.iaea.org/Search/search.aspx?orig_q=RN:20038756 (1988).
14. Singwi, K. S., Sjölander, A. Diffusive motions in water and cold neutron scattering. *Physical Review.* **119** (3), 863-871 (1960).
15. Sears, V. F. Theory of cold neutron scattering by homonuclear diatomic liquids: i. free rotation. *Canadian Journal of Physics.* **44** (6), 1279-1297 (1966).
16. Sears, V. F. Theory of cold neutron scattering by homonuclear liquid: ii. hindered rotation. *Canadian Journal of Physics.* **44** (6), 1299-1311 (1966).

17. Schirò, G. et al. Translational diffusion of hydration water correlates with functional motions in folded and intrinsically disordered proteins. *Nature Communications.* **6**, 6490 (2015).

18. Grimaldo, M. et al. Hierarchical molecular dynamics of bovine serum albumin in concentrated aqueous solution below and above thermal denaturation. *Physical Chemistry Chemical Physics.* **17** (6), 4645-4655 (2015).

19. Eanes, E. D., Glenner, G. G. X-ray diffraction studies on amyloid filaments. *Journal of Histochemistry & Cytochemistry.* **16** (11), 673-677 (1968).

20. Bonar, L., Cohen, A. S., Skinner, M. M. Characterization of the Amyloid Fibril as a Cross-β Protein. *Proceedings of the Society for Experimental Biology and Medicine.* **131** (4), 1373-1375 (1969).

21. Chiti, F., Dobson, C. M. Protein Misfolding, Amyloid Formation, and Human Disease: A Summary of Progress Over the Last Decade. *Annual Review of Biochemistry.* **86** (1), 27-68 (2017).

22. Knowles, T. P. J., Vendruscolo, M., Dobson, C. M. The amyloid state and its association with protein misfolding diseases. *Nature Reviews Molecular Cell Biology.* **15** (6), 384-396 (2014).

23. Maji, S. K. et al. Functional amyloids as natural storage of peptide hormones in pituitary secretory granules. *Science.* **325** (5938), 328-332 (2009).

24. Li, J. et al. The RIP1/RIP3 necrosome forms a functional amyloid signaling complex required for programmed necrosis. *Cell.* **150** (2), 339-350 (2012).

25. Knowles, T. P. J., Mezzenga, R. Amyloid fibrils as building blocks for natural and artificial functional materials. *Advanced Materials.* **28** (31), 6546-6561 (2016).

26. Stephens, A. D., Kaminski Schierle, G. S. The role of water in amyloid aggregation kinetics. *Current Opinion in Structural Biology.* **58**, 115-123 (2019).

27. Adamcik, J., Mezzenga, R. Amyloid polymorphism in the protein folding and aggregation energy landscape. *Angewandte Chemie International Edition.* **57** (28), 8370-8382 (2018).

28. Liu, Z., et al. Entropic contribution to enhanced thermal stability in the thermostable P450 CYP119. *Proceedings of the National Academy of Sciences of the United States of America.* **115** (43), E10049-E10058 (2018).

29. Coquelle, N. et al. Chromophore twisting in the excited state of a photoswitchable fluorescent protein captured by time-resolved serial femtosecond crystallography. *Nature Chemistry.* **10** (1), 31-37 (2018).

30. Henzler-Wildman, K. A., et al. A hierarchy of timescales in protein dynamics is linked to enzyme catalysis. *Nature.* **450** (7171), 913-916 (2007).

31. Fichou, Y. et al. Hydration water mobility is enhanced around tau amyloid fibers. *Proceedings of the National Academy of Sciences of the United States of America.* **112** (20), 6365-6370 (2015).

32. Burns, J., Pennock, C. A., Stoward, P. J. The specificity of the staining of amyloid deposits with thioflavine T. *The Journal of Pathology and Bacteriology.* **94** (2), 337-344 (1967).

33. Iqbal, K., Liu, F., Gong, C.-X., Grundke-Iqbal, I. Tau in Alzheimer disease and related tauopathies. *Current Alzheimer Research.* **7** (8), 656-664 (2010).

34. Krężel, A., Bal, W. A formula for correlating pKa values determined in D2O and H2O. *Journal of Inorganic Biochemistry.* **98** (1), 161-166 (2004).

35. Dolman, M., Halling, P. J., Moore, B. D., Waldron, S. How dry are anhydrous enzymes? Measurement of residual and buried 18O-labeled water molecules using mass spectrometry. *Biopolymers.* **41** (3), 313-321 (1997).

36. Pounot, K. *kpounot/nPDyn: v3.0.0.* Zenodo. (2021).

37. Yi, Z., Miao, Y., Baudry, J., Jain, N., Smith, J. C. Derivation of mean-square displacements for protein dynamics from elastic incoherent neutron scattering. *Journal of Physical Chemistry B.* **116** (16), 5028-5036 (2012).

38. Peters, J., Kneller, G. R. Motional heterogeneity in human acetylcholinesterase revealed by a non-Gaussian model for elastic incoherent neutron scattering. *The Journal of Chemical Physics.* **139** (16), 165102 (2013).

39. Zeller, D., Telling, M. T. F., Zamponi, M., García Sakai, V., Peters, J. Analysis of elastic incoherent neutron scattering data beyond the Gaussian approximation. *The Journal of Chemical Physics.* **149** (23), 234908 (2018).

40. Roosen-Runge, F., Seydel, T. A generalized mean-squared displacement from inelastic fixed window scans of incoherent neutron scattering as a model-free indicator of anomalous diffusion confinement. *EPJ Web of Conferences.* **83**, 02015 (2015).

41. Ortega, A., Amorós, D., García de la Torre, J. Prediction of hydrodynamic and other solution properties of rigid proteins from atomic- and residue-level models. *Biophysical Journal.* **101** (4), 892-898 (2011).

42. Hennig, M., Frick, B., Seydel, T., IUCr Optimum velocity of a phase-space transformer for cold-neutron backscattering spectroscopy. *Journal of Applied Crystallography.* **44** (3), 467-472 (2011).

43. Paalman, H. H., Pings, C. J. Numerical evaluation of X-ray absorption factors for cylindrical samples and annular sample cells. *Journal of Applied Physics.* **33** (8), 2635-2639 (1962).

44. Ow, S.-Y., Dunstan, D. E. The effect of concentration, temperature and stirring on hen egg white lysozyme amyloid formation. *Soft Matter.* **9** (40), 9692-9701 (2013).

45. Tominaga, T., Sahara, M., Kawakita, Y., Nakagawa, H., Yamada, T. Evaluation of sample cell materials for aqueous solutions used in quasi-elastic neutron scattering measurements. *Journal of Applied Crystallography.* **54** (6), 1631-1640 (2021).

46. Beck, C. et al. Following protein dynamics in real time during crystallization. *Crystal Growth & Design.* **19** (12), 7036-7045 (2019).

47. Smith, A. A., Testori, E., Cadalbert, R., Meier, B. H., Ernst, M. Characterization of fibril dynamics on three timescales by solid-state NMR. *Journal of Biomolecular NMR.* **65** (3-4), 171-191 (2016).

48. Wang, T., Jo, H., DeGrado, W. F., Hong, M. Water distribution, dynamics, and interactions with Alzheimer's β-amyloid fibrils investigated by solid-state NMR. *Journal of the American Chemical Society.* **139** (17), 6242-6252 (2017).

49. Rezaei-Ghaleh, N., Giller, K., Becker, S., Zweckstetter, M. Effect of zinc dinding on β-amyloid structure and dynamics: Implications for Aβ aggregation. *Biophysical Journal.* **101** (5), 1202-1211 (2011).

50. Vugmeyster, L., et al. Fast motions of key methyl groups in amyloid-β fibrils. *Biophysical Journal.* **111** (10), 2135-2148 (2016).

51. Yang, X., Wang, B., Hoop, C. L., Williams, J. K., Baum, J. NMR unveils an N-terminal interaction interface on acetylated-α-synuclein monomers for recruitment to fibrils. *Proceedings of the National Academy of Sciences of the United States of America.* **118** (18), e2017452118 (2021).

52. Tuttle, M. D. et al. Solid-state NMR structure of a pathogenic fibril of full-length human α-synuclein. *Nature Structural & Molecular Biology.* **23** (5), 409-415 (2016).

53. Karamanos, T. K., Kalverda, A. P., Thompson, G. S., Radford, S. E. Mechanisms of amyloid formation revealed by solution NMR. *Progress in Nuclear Magnetic Resonance Spectroscopy.* **88 - 89**, 86-104 (2015).

54. Lai, Y.-C., Kuo, Y.-H., Chiang, Y.-W. Identifying protein conformational dynamics using spin-label ESR. *Chemistry - An Asian Journal.* **14** (22), 3981-3991 (2019).

55. Franck, J. M., Han, S. Overhauser dynamic nuclear polarization for the study of hydration dynamics, explained. *Methods in Enzymology.* **615**, 131-175 (2019).

56. Pavlova, A., et al. Protein structural and surface water rearrangement constitute major events in the earliest aggregation stages of tau. *Proceedings of the National Academy of Sciences of the United States of America.* **113** (2), E127-E136 (2016).

57. Lin, Y. et al. Liquid-liquid phase separation of tau driven by hydrophobic interaction facilitates fibrillization of tau. *bioRxiv.* 2020.08.05.237966 (2020).

58. Decatur, S. M. Elucidation of residue-level structure and dynamics of polypeptides via isotope-edited infrared spectroscopy. *Accounts of Chemical Research.* **39** (3), 169-175 (2006).

59. Chatani, E., Tsuchisaka, Y., Masuda, Y., Tsenkova, R. Water molecular system dynamics associated with amyloidogenic nucleation as revealed by real time near infrared spectroscopy and aquaphotomics. *PLoS One.* **9** (7), e101997 (2014).

60. Goret, G., Aoun, B., Pellegrini, E. MDANSE: An interactive analysis environment for molecular dynamics simulations. *Journal of Chemical Information and Modeling.* **57** (1), 1-5 (2017).

61. Fujiwara, S. et al. Internal dynamics of a protein that forms the amyloid fibrils observed by neutron scattering. *Journal of the Physical Society of Japan.* **82** (Suppl A), SA019 (2013).

62. Schiró, G., et al. Neutron scattering reveals enhanced protein dynamics in concanavalin a amyloid fibrils. *Journal of Physical Chemistry Letters.* **3** (8), 992-996 (2012).

63. Pounot, K. et al. Zinc determines dynamical properties and aggregation kinetics of human insulin. *Biophysical Journal.* **120** (5), 886-898 (2021).

64. Fujiwara, S. et al. Dynamic properties of human α-synuclein related to propensity to amyloid fibril formation. *Journal of Molecular Biology.* **431** (17), 3229-3245 (2019).

65. Sanz, A. et al. High-pressure cell for simultaneous dielectric and neutron spectroscopy. *Review of Scientific Instruments.* **89** (2), 023904 (2018).

66. Adams, M. A., et al. Simultaneous neutron scattering and Raman scattering. *Applied Spectroscopy.* **63** (7), 727-732 (2009).